

Abstract

The role that continental margin sediments play in the global carbon cycle and the mitigation of climate change is currently not well understood. Recent research has indicated that these sediments might store large amounts of organic carbon; however, Blue Carbon research continues to focus on vegetated coastal ecosystems as actionable Blue Carbon. Marine sediments are considered emerging Blue Carbon ecosystems, but to decide whether they are actionable requires better quantifications of organic carbon stocks, accumulation rates, and the mitigation potential from avoided emissions. To close some of these knowledge gaps, we spatially predicted organic carbon content, dry bulk density and sediment accumulation rates across the Norwegian margin. The resulting predictions were used to estimate organic carbon stocks in surface sediments and their accumulation rates. We found that organic carbon stocks are two orders of magnitude higher than those of vegetated coastal ecosystems and comparable to terrestrial ecosystems in Norway. Accumulation rates of organic carbon are spatially highly variable and linked to geomorphology and associated sedimentary processes. We identify shelf valleys with a glacial origin as hotspots of organic carbon accumulation with a potentially global role due to their widespread occurrence on formerly glaciated continental margins. The complex and heterogenous nature of continental margins regarding organic carbon accumulation means that to close existing knowledge gaps requires detailed spatial predictions that account for those complexities. Only in this way will it be possible to evaluate whether margin sediments might be actionable Blue Carbon ecosystems.

Plain Language Summary

To keep global average temperature rise well below 2°C requires drastic emission reductions and a removal of carbon dioxide from the atmosphere. Part of the carbon dioxide removal could be achieved by nature itself, if ecosystems that remove substantial amounts of carbon from the atmosphere are protected, managed, or restored. In the marine environment, the focus has been placed on coastal ecosystems with rooted vegetation, as they remove carbon at high rates, are threatened by human activities and are amenable to management. Collectively, these are called actionable Blue Carbon ecosystems. More recently, marine sediments have been put forward, but these are currently labelled emerging Blue Carbon ecosystems due to existing knowledge gaps. To close some of these gaps we mapped the amount of organic carbon stored in sediments of the Norwegian seafloor and the rates at which it is accumulated. We found that there is 100 times more organic carbon in the seabed than in vegetated coastal ecosystems in Norway. Rates of organic carbon accumulation vary in space and are highest in glacial troughs. To improve our estimates of how much carbon accumulates in marine sediments globally will require to consider the complex nature of the continental margins.

55

56 **1 Introduction**

57 The burial of organic carbon in seafloor sediments is crucial for moving carbon from the short-
58 term surface to the long-term geological cycle (Keil, 2017). This long-term carbon cycle is, in
59 turn, controlling the concentration of atmospheric carbon dioxide (CO₂) over geological
60 timescales (Bernier, 2003). The size of the organic carbon seafloor sink, and the relative
61 contributions of the continental margins versus the deep-sea, have been a matter of research for
62 the last 50 years or so. A first estimate, based on multiplying average organic carbon content of
63 Holocene sediments by area and thickness, yielded 223 Tg C yr⁻¹, of which 10% and 88% are
64 deposited on the continental shelf and slope, respectively (Gershanovich et al., 1974; cited in
65 Hedges & Keil, 1995). Bernier (1982) argued that organic carbon is preferentially buried in
66 deltaic shelf sediments (83% of a total burial rate of 126 Tg C yr⁻¹). His estimates were
67 subsequently revised by Hedges & Keil (1995) to account for organic carbon burial in sediments
68 of the continental shelves and upper slopes, respectively, and estimated that roughly 90 % of
69 organic carbon is buried in coastal and continental margin settings.

70 Routine collection of ocean colour data with satellites has made it possible to estimate primary
71 production, particle export, bottom flux, and burial of organic carbon with spatial detail. Muller-
72 Karger et al. (2005) estimated that continental margins may be responsible for >40% of the
73 organic carbon sequestration in the ocean. An even higher estimate of 98% for margins was
74 published by Dunne et al. (2007). The same authors also estimated that 85% of the total burial
75 flux (0.67 ± 0.45 Pg C yr⁻¹) occurred on continental shelves (shallower than 200 m). The latter,
76 however, is in contradiction to de Haas et al. (2002) suggesting that shelf areas do not
77 accumulate substantial amounts of organic carbon under present day conditions and, only locally,
78 are considerable amounts of organic carbon buried. De Haas et al. (2002) concluded that the role
79 of shelves as sinks for organic carbon is overestimated due to recurrent hydrodynamic processes
80 that prevent its deposition in comparison to deeper continental slopes.

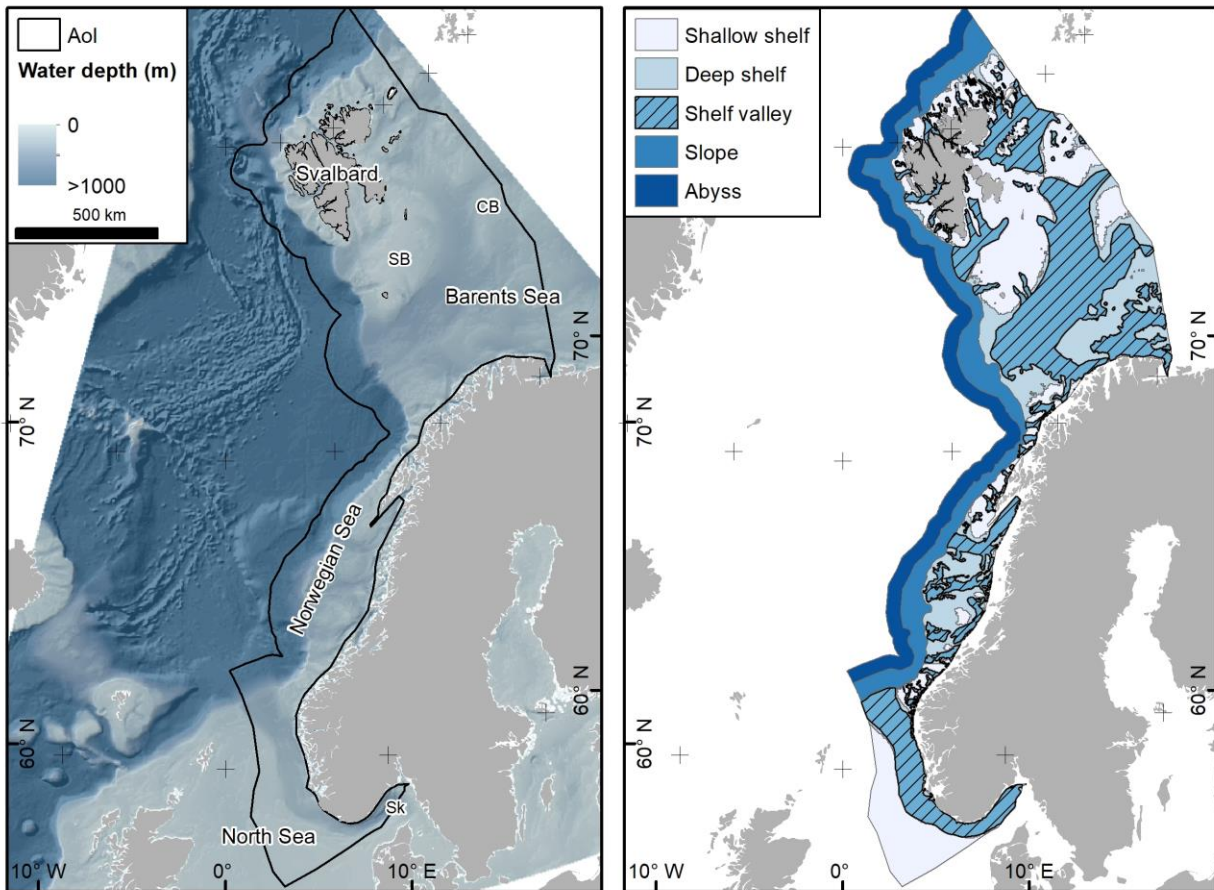
81 More recently, it has been claimed that the importance of seafloor sediments as places of organic
82 carbon sequestration is somewhat diminished in comparison to vegetated coastal ecosystems
83 (saltmarshes, mangroves, and seagrass meadows), which would account for 46% of the marine
84 organic carbon burial despite covering only 0.2% of the ocean surface (Duarte et al., 2005,
85 2013). Vegetated coastal ecosystems have been a focus of research over the last ten to fifteen
86 years under the concept of Blue Carbon (Nellemann et al., 2009). As these ecosystems might be
87 able to remove CO₂ from the atmosphere at high rates, store fixed CO₂ as organic carbon over
88 timescales of centuries or longer, and are frequently threatened by human activities, it has been
89 suggested that management, conservation, and restoration of vegetated coastal ecosystems might
90 significantly contribute to greenhouse gas removal from the atmosphere (Lovelock & Duarte, 2019).
91 Other ecosystems might satisfy the above definition of actionable Blue Carbon, but research gaps
92 currently preclude from a classification as such. Emerging Blue Carbon ecosystems include wild
93 and cultivated macroalgae, unvegetated tidal flats, and marine sediments (Howard et al., 2023).
94 Continental shelf and slope (margin) sediments might exhibit lower organic carbon stocks and
95 accumulation rates per unit area but cover much larger areas than vegetated coastal ecosystems.
96 The large spatial extent might weigh out the low areal stocks and accumulation rates, but the
97 importance of continental margins as places of organic carbon accumulation and storage relative
98 to vegetated coastal ecosystems is currently not well understood. While our knowledge on local,
99 regional, and global organic carbon stocks has steeply increased over the past few years (Atwood
100 et al., 2020; Diesing et al., 2017, 2021; Hunt et al., 2020; Lee et al., 2019; Legge et al., 2020;
101 Smeaton et al., 2021; Wilson et al., 2018), there currently exist knowledge gaps regarding

102 organic carbon accumulation in margin sediments. Specifically, we lack spatially explicit
103 quantifications of organic carbon accumulation rates and related uncertainties in the estimates.
104 Such knowledge gaps could be filled with the application of machine learning spatial models, as
105 exemplified by Diesing et al. (2021). Accounting for the complex nature of continental margins
106 with zones of rapid carbon cycling and accumulation juxtaposed (Diesing et al., 2021; de Haas et
107 al., 2002) will be an important consideration.

108 This study investigates the significance of continental margin sediments in terms of organic
109 carbon accumulation and storage potential. We do not aim to estimate organic carbon burial, as
110 the reference depths below which organic carbon is assumed to be removed from the short-term
111 surface carbon cycle vary between studies and organic carbon might not even be irreversibly
112 buried or preserved (Bradley et al., 2022). Instead, we estimate the amount of organic carbon that
113 accumulates in the seabed on a timescale of approximately 100 - 150 years. Specifically, we aim
114 to answer how much organic carbon is accumulated and stored in surface sediments (0 – 10 cm)
115 on the Norwegian continental margin and discuss its hotspot potential for carbon storage in
116 contrast to vegetated coastal ecosystems and terrestrial ecosystems.

117 1.1 Study site

118 Our area of interest (Figure 1) comprises the Norwegian continental shelf and slope (after Harris
119 et al., 2014), which we define here as the Norwegian continental margin. We also include
120 shallow parts of the abyss (deep sea) within 50 km distance from the seaward boundary of the
121 slope to make best use of existing data. We further subdivide the continental shelf into shallow
122 shelf (above 200 m water depth), deep shelf (between 200 m water depth and the shelf break)
123 and shelf valleys (irrespective of water depth), as mapped by Harris et al. (2014). On the
124 formerly glaciated continental margin of Norway, most shelf valleys are of glacial origin and as
125 such could also be considered as glacial troughs. Our study site spans 26° of latitude and
126 approximately 3000 km between the North Sea and the Arctic Ocean north off Svalbard.



127
 128 **Figure 1.** Overview of the area of interest (AoI): Left – Water depth (GEBCO Bathymetric
 129 Compilation Group, 2019), regional seas and locations mentioned in the text. CB – Central Bank,
 130 SB – Spitsbergen Bank, Sk – Skagerrak. Right – Geomorphological units based on Harris et al.
 131 (2014). The continental shelf is further subdivided into shallow shelf (0 to 200 m water depth)
 132 and deep shelf (200 m depth to the shelf edge).

133 2 Data

134 2.1 Response variables

135 To derive organic carbon stocks and accumulation rates it is necessary to spatially predict dry
 136 bulk density, organic carbon content, and sediment accumulation rates (also referred to as linear
 137 sedimentation rates). Several studies have shown that an important predictor for organic carbon
 138 content is the silt-clay (mud) content in seafloor sediments (Diesing et al., 2017; Wilson et al.,
 139 2018). As this important predictor layer did not exist in the area of interest, we spatially
 140 predicted it. We also predicted the spatial distribution of substrate types and the depositional
 141 environments and used the class probabilities as predictors. Substrate type is potentially an
 142 important predictor for mud content, dry bulk density, and organic carbon content, while the
 143 depositional environment might be important to predict sedimentation rates. Table 1 summarises
 144 the variables that have been estimated, how they were derived, and how they were used in the
 145 process we describe.

146

147 **Table 1.** Overview of variables that were estimated, how they were derived and how they were
 148 used. Reference is also made to the respective figures and repositories.
 149

<i>Variable</i>	<i>Derived by</i>	<i>Used</i>	<i>Figure</i>	<i>Repository</i>
<i>Substrate type</i>	Spatial prediction	As predictor variable	S1	Zenodo
<i>Depositional environment</i>	Spatial prediction	As predictor variable	S2	Zenodo
<i>Mud content</i>	Spatial prediction	As predictor variable	S3	Zenodo
<i>Dry bulk density</i>	Spatial prediction	To calculate organic carbon stocks and accumulation rates	S4	Zenodo
<i>Organic carbon content</i>	Spatial prediction	To calculate organic carbon stocks and accumulation rates	S5	Zenodo
<i>Sediment accumulation rate</i>	Spatial prediction	To calculate organic carbon accumulation rates	S6	Zenodo
<i>Organic carbon stock</i>	Calculation (eq. 2)	For analysis	2	Pangaea
<i>Organic carbon accumulation rate</i>	Calculation (eq. 4)	For analysis	4	Pangaea

150

151 2.1.1 Substrate type and depositional environment

152 Maps of substrate type and depositional environment are routinely produced by expert
 153 interpretation at local, regional and overview scales as part of the Mareano seafloor mapping
 154 programme (www.mareano.no/en). However, these maps currently cover only a fraction of the
 155 Norwegian margin (Figures S1 and S2). We therefore decided to fill the existing coverage gaps
 156 by spatial prediction. We treated the existing maps as response data by converting the polygon
 157 shapefiles into raster data with a resolution of 4 km aligned to the predictor raster stack (see
 158 chapter 2.2 for details) using the Polygon to Raster function in ArcGIS 10.8.2, with maximum
 159 combined area as cell assignment type. The raster datasets were subsequently converted into
 160 point data (Raster to Point function) with the substrate type or depositional environment class as
 161 attribute. The original classifications contained more than 30 substrate types and six classes of
 162 depositional environment. These were simplified to eight substrate types and three classes of
 163 depositional environment, respectively (Table S1 and S2).

164 2.1.2 Mud content

165 Grain-size data (mud, sand, and gravel content) were obtained from the PANGAEA database
 166 (Felden et al., 2023), the ICES Data Portal contaminants dataset (<https://data.ices.dk/>), the
 167 Environmental Monitoring database MOD (DNV, 2023), the Geological Survey of Norway and
 168 the Mareano chemistry database (<https://mareano.no/en/maps-and-data/chemical-data>). Data
 169 were pre-processed by replacing records of 0 weight-% with 0.001 weight-% and rescaling to
 170 achieve fraction sums of 100 weight-% (Martín-Fernández & Thió-Henestrosa, 2006). This was
 171 necessary as additive log-ratios (Pawlowsky-Glahn & Olea, 2004) were subsequently calculated
 172 due to the compositional nature of the grain-size data.

173 2.1.3 Dry bulk density

174 Dry bulk density data were obtained from the PANGAEA database via a data warehouse query.
 175 The downloaded data were restricted to the upper 0.5 m of the sediment column. Furthermore,

176 we used data on mud content from the Mareano chemistry database to calculate porosity (ϕ)
177 according to an empirical equation (Jenkins, 2005) and ultimately dry bulk density (ρ_d)
178 according to $\rho_d = (1 - \phi)\rho_s$ with grain density, $\rho_s = 2.65 \text{ g cm}^{-3}$.

179 *2.1.4 Organic carbon content and sediment accumulation rates*

180 Data on organic carbon content and ^{210}Pb -derived sediment accumulation rates were obtained
181 from the MOSAIC database (Paradis et al., 2023; van der Voort et al., 2020). The datasets
182 included data from the Mareano chemistry database among others.

183 *2.1.5 Pseudo samples*

184 Datasets compiled from the literature or obtained from databases are frequently biased. For
185 example, sediment accumulation rates are usually only reported in areas where sediments are
186 deposited and caution is advised when spatially predicting such data (Jenkins, 2018). One
187 strategy to deal with this limitation is to include pseudo-observations (Hengl et al., 2017); in this
188 case records of 0 cm yr^{-1} sediment accumulation in areas that are erosional in nature. Similar
189 approaches have previously been adopted by Diesing et al. (2021) and Mitchell et al. (2021). We
190 randomly placed pseudo samples within the area predicted as Erosion or Transport (Figure S2).
191 Additionally, we observed that coarse-grained sediments (muddy sandy gravel, sandy gravel, and
192 gravel) were under-represented in our datasets. We therefore included a limited number ($n <$
193 100) of stations where these sediments had been observed and randomly assigned a sediment
194 composition adhering to their class definitions (Folk, 1954). These pseudo-observations were
195 used in the grain-size and dry bulk density datasets.

196 **2.2 Predictors variables**

197 We created a raster stack of predictor variables that we considered potentially relevant for
198 predicting the response variables and that were available with (near) full coverage in the area of
199 interest at a sufficiently high spatial resolution. The resolution that was finally chosen was 4 km,
200 which translates to a map scale of approximately 1 : 8,000,000 according to a recommended
201 formula in Hengl (2006). The raster stack was projected to the Lambert azimuthal equal area
202 projection.

203 We included variables on seafloor terrain (bathymetry, topographic position, distance to nearest
204 shoreline), ocean colour (chlorophyll-a, primary production and suspended particulate matter),
205 biogeochemistry (surface partial pressure of CO_2 , dissolved molecular oxygen of bottom water),
206 sea ice concentration, bottom fishing intensity (swept area ratio), and oceanography (current
207 speed, temperature, and salinity). Multi-annual statistics (mean, minimum, maximum, and range)
208 were calculated for most predictors (Table S3).

209 **3 Methods**

210 **3.1 Spatial predictions**

211 **3.1.1 Machine learning algorithms**

212 We chose the random forest (RF) algorithm (Breiman, 2001) to spatially predict the response
213 variables substrate type, depositional environment, and mud content. Further, we use the quantile
214 regression forest (QRF) algorithm (Meinshausen, 2006) to make spatial predictions of the

215 response variables dry bulk density, organic carbon content and ^{210}Pb -derived sediment
 216 accumulation rates. QRF can be seen as an extension of the RF algorithm, which has shown high
 217 predictive accuracy in several studies across various research domains (Huang et al., 2014;
 218 Mutanga et al., 2012; Oliveira et al., 2012; Prasad et al., 2006). RF can be used for both
 219 classification and regression modelling, while QRF deals only with regression tasks. RF is an
 220 ensemble technique that grows many trees and aggregates the majority class (classification) or
 221 conditional mean (regression) from each tree in a forest to make an ensemble prediction. QRF
 222 also returns the whole conditional distribution of the response variable, based on which other
 223 measures of central tendency (e.g., median) and of prediction uncertainty can be obtained.
 224 Following common practice in the global soil mapping community (Arrouays et al., 2014;
 225 Heuvelink, 2014), we used the 90 % prediction interval (PI90) as a measure of spatially explicit
 226 uncertainty. PI90 gives the range of values within which the true value is expected to occur nine
 227 times out of ten, with a one in 20 probability for each of the two tails (Arrouays et al., 2014). It is
 228 defined as

$$229 \quad \mathbf{PI90} = \mathbf{q_{0.95}} - \mathbf{q_{0.05}} \quad (1)$$

230 with $q_{0.95}$ and $q_{0.05}$ being the 0.95 and 0.05 quantiles of the distribution, respectively. We
 231 chose the median as a measure of central tendency, as the conditional distributions are most
 232 likely non-normal, and the median is not affected by extreme outliers.

233 3.1.2 Pre-processing

234 Prior to modelling, the predictor raster stack was cropped to the area of interest. Areas mapped as
 235 “Rock and boulders” in the substrate type model were excluded from further analysis, as we are
 236 only interested in the sedimentary environment. The datasets of the response variables organic
 237 carbon content and dry bulk density included information on depth below seabed. These datasets
 238 were filtered to only include records between 0 cm and 10 cm depth. The response data were
 239 averaged in those cases where more than one value was falling into a grid cell of the predictor
 240 stack.

241 3.1.3 Predictor variable selection

242 Although it is prudent to initially select a wide range of predictors, it is generally recommended
 243 to limit the number of predictors that are finally used for modelling. This is especially true when
 244 the number of records in the response data set is low. Variable selection can be achieved in
 245 different ways. Here we chose forward feature (variable) selection as implemented in the
 246 package CAST (Meyer et al., 2018). The algorithm first trains models based on all possible
 247 combinations of two predictor variables. The best combination is retained and tested for the best
 248 performance with a third variable. Additional variables are added until the performance stops
 249 improving. The model performance was calculated as R^2 using a spatial cross-validation scheme
 250 (see below). Prior to forward feature selection, a predictor variable pre-selection was executed to
 251 limit processing time. This pre-selection process initially only retained important variables that
 252 performed better than random variables using the Boruta algorithm (Kursa & Rudnicki, 2010). In
 253 the second step of the variable pre-selection, a de-correlation analysis was carried out to limit the
 254 collinearity. This was achieved with the *vifcor* function of the package *usdm* (Naimi et al., 2014).
 255 The function requires a correlation threshold and the predictor variables as input to calculate the
 256 variance inflation factor (VIF). The correlation threshold was stepwise decreased from 1 with a

257 step size of 0.01 until the VIF was below 2.5 to avoid a problematic amount of collinearity
258 (Johnston et al., 2018).

259 3.1.4 Model performance

260 Model performance needs to be estimated for model tuning, variable selection, and model
261 validation. Model performance estimation is frequently based on k-fold cross validation,
262 whereby the response data are split into k folds, a model is built on k – 1 folds, and validated
263 against the fold which was not used for model building. This process is repeated k times. In
264 standard, non-spatial machine learning applications, this k-fold split is performed randomly on
265 the response data. However, this is not appropriate in the case of spatial data as spatial
266 autocorrelation might lead to inflated estimates of model performance (Ploton et al., 2020;
267 Roberts et al., 2017). Folds therefore need to be spatially separated and this was achieved with
268 the function *cv_spatial* of the package *blockCV* (Valavi et al., 2019). Block size was initially
269 determined by estimating the spatial autocorrelation range of the response data with the *automap*
270 package (Hiemstra et al., 2009). The distance functions of the sample-to-sample, prediction-to-
271 sample, and cross validation distances were plotted with the *plot_geodist* function of *CAST*
272 (Meyer & Pebesma, 2021) and the block size altered by applying a multiplier to the spatial
273 autocorrelation range until there was a visual agreement between the distance functions of the
274 prediction-to-sample and cross validation distances.

275 The performance of the final regression models (mud content, dry bulk density, organic carbon
276 content and sediment accumulation rate) was assessed based on the explained variance (R^2) and
277 the root mean square error (RMSE). The performance of the classification models (Substrate
278 type and Depositional environment) was assessed with the overall accuracy (Congalton, 1991)
279 and the balanced error rate (BER, Luts et al., 2010), which is the average of the proportion of
280 wrong classifications in each class, thereby accounting for class imbalances.

281 3.1.5 Area of applicability

282 Although it is technically possible to predict the response variable over the full extent of the
283 predictor variables, such predictions might be unreliable where they extrapolate beyond the
284 predictor variable space that has been captured by the model (Meyer & Pebesma, 2021, 2022). It has
285 therefore been suggested to estimate the area of applicability (AOA) of a model, where the
286 combination of predictor variables is similar to what the model has been trained with. This can
287 be achieved with the *aoa* function of the package *CAST* (Meyer et al., 2023).

288 3.1.6 Qualitative evaluation

289 Additionally, we used expert judgement to evaluate whether the predicted patterns were
290 reasonable by comparing them with existing maps and a general understanding of the involved
291 processes and their products. Although such an assessment is qualitative and somewhat
292 subjective, it is currently the only way to incorporate expert knowledge and we consider it an
293 essential part of the mapping process.

294 3.2 Calculation of organic carbon stocks

295 Organic carbon stocks (OCS) are calculated by multiplying the predicted organic carbon contents
296 (G) with the predicted dry bulk densities (ρ_d) and the sediment thickness ($d = 0.1$ m):

$$297 \quad \mathbf{OCS} \ (\mathbf{kg} \ \mathbf{m}^{-2}) = \frac{\mathbf{G} \ (\%)}{100} \cdot \mathbf{1000} \cdot \mathbf{\rho}_d \ (\mathbf{g} \ \mathbf{cm}^{-3}) \cdot \mathbf{d} \ (\mathbf{m}) \quad (2)$$

298 Calculations were carried out for the whole area and limited to the joint AOA of the organic
299 carbon and dry bulk density models.

300 The total reservoir size mOC was calculated by summing OCS of all pixels and multiplying with
301 the area of one pixel ($A = 16,000,000 \text{ m}^2$):

$$302 \quad \mathbf{m}_{oc}(\mathbf{Tg}) = (\mathbf{A}(\mathbf{m}^2) \cdot \sum \mathbf{OCS} \ (\mathbf{kg} \ \mathbf{m}^{-2}))/\mathbf{1,000,000,000} \quad (3)$$

303 3.3 Calculation of organic carbon accumulation rates

304 Organic carbon accumulation rates (OCAR) are calculated by multiplying organic carbon
305 contents (0 – 10 cm) with dry bulk densities and sediment accumulation rates (ω):

$$306 \quad \mathbf{OCAR} \ (\mathbf{g} \ \mathbf{m}^{-2} \ \mathbf{yr}^{-1}) = \frac{\mathbf{G} \ (\%)}{100} \cdot \mathbf{\rho}_d \ (\mathbf{g} \ \mathbf{cm}^{-3}) \cdot \mathbf{\omega} \ (\mathbf{cm} \ \mathbf{yr}^{-1}) \cdot \mathbf{10,000} \quad (4)$$

307 Calculations were carried out for the whole area and limited to the joint AOA of the organic
308 carbon, dry bulk density and sediment accumulation rate models.

309 The total mass of organic carbon that is accumulated annually (OCA) is calculated by summing
310 OCAR of all pixels and multiplying with the area of one pixel ($A = 16,000,000 \text{ m}^2$):

$$311 \quad \mathbf{OCA}(\mathbf{Tg} \ \mathbf{yr}^{-1}) = (\mathbf{A}(\mathbf{m}^2) \cdot \sum \mathbf{OCAR} \ (\mathbf{g} \ \mathbf{m}^{-2} \ \mathbf{yr}^{-1}))/\mathbf{1,000,000,000,000} \quad (5)$$

312 3.4 Propagation of uncertainties

313 Uncertainties were propagated by taking the square root of the sum of squared relative
314 uncertainties:

$$315 \quad \mathbf{\delta OCS} = \mathbf{OCS} \cdot \sqrt{\left(\frac{\mathbf{\delta G}}{\mathbf{G}}\right)^2 + \left(\frac{\mathbf{\delta \rho}_d}{\mathbf{\rho}_d}\right)^2} \quad (6)$$

$$316 \quad \mathbf{\delta OCAR} = \mathbf{OCAR} \cdot \sqrt{\left(\frac{\mathbf{\delta G}}{\mathbf{G}}\right)^2 + \left(\frac{\mathbf{\delta \rho}_d}{\mathbf{\rho}_d}\right)^2 + \left(\frac{\mathbf{\delta \omega}}{\mathbf{\omega}}\right)^2} \quad (7)$$

317 The symbol δ signifies the uncertainty of a quantity.

318 4 Results and discussion

319 4.1 Model Performance

320 The characteristics and performance indicators of the six spatial models are summarised in Table
321 2. It is important to stress that the performance indicators were derived in a spatial cross-
322 validation scheme and were expected to be lower than those derived from random cross-
323 validation, which was frequently employed in previous studies. Despite this, our model on
324 organic carbon content explains 77% of the variance in the data. This is comparable to studies
325 which did not employ spatial cross-validation (Atwood et al., 2020; Diesing et al., 2017; Lee et
326 al., 2019). The mud content model had a similar R^2 value of 0.76, higher than those of previously
327 published models (Mitchell et al., 2019; Stephens & Diesing, 2015; Wilson et al., 2018). The dry
328 bulk density model explained 70% of the variance. This is, to our knowledge, the first published
329 model on this seafloor sediment property. The model for sediment accumulation rates performed

330 somewhat poorer, explaining 32% of the variance. Previous studies have shown that predicting
 331 sediment accumulation rates with machine learning can be challenging (e.g., Mitchell et al.,
 332 2021). However, based on a comparison with published maps (Bøe et al., 1996; de Haas et al.,
 333 1997; Pathirana et al., 2014) and our expert judgement, we conclude that the overall patterns of
 334 sediment accumulation (Fig. S6) are reasonable. The model on the depositional environment
 335 performed well with an overall accuracy of 81% and a balanced error rate of 0.28. The lower
 336 performance of the substrate type model might be attributable to the higher number of classes
 337 (eight vs three).

338 This is one of the first marine studies that employed the concept of the area of applicability
 339 (Meyer & Pebesma, 2021). All models had areas of applicability larger than 80% of the total
 340 area, two of them (substrate type and organic carbon content) even >90%. The resulting maps
 341 (Figures 2-3, S1-S6) are therefore applicable to at least 80% of the area of interest.

342

343 **Table 2.** Summary of the six models and their performance. Model types: RF- Random Forest;
 344 QRF – Quantile Regression Forest. BER – Balanced Error Rate. RMSE – Root Mean Squared
 345 Error. AOA – Area of Applicability.

346

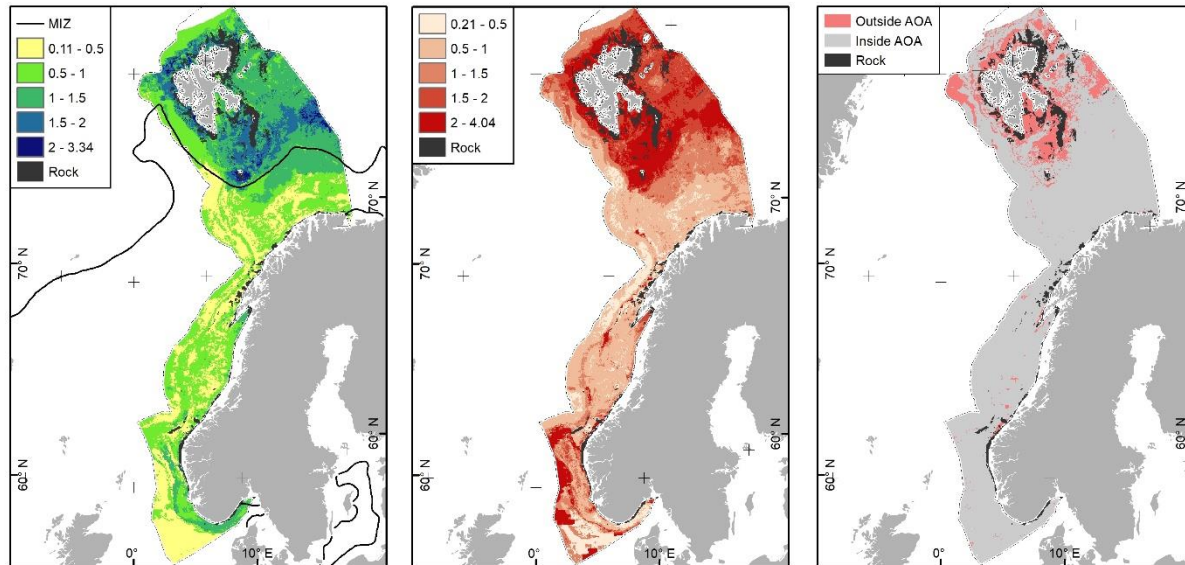
<i>Response variable</i>	Type	Unit	Number of samples	Number of predictors	Model	Accuracy	BER	RMSE	R ²	AOA (% of total area)
<i>Substrate type</i>	categorical	-	23798	9	RF	0.59	0.53	-	-	91.22
<i>Depositional environment</i>	categorical	-	13305	9	RF	0.81	0.28	-	-	88.02
<i>Mud content¹</i>	continuous	weight -%	4531	9	RF	-	-	1.456	0.76	81.53
<i>Dry bulk density</i>	continuous	g cm ⁻³	606	10	QRF	-	-	0.192	0.70	88.57
<i>Organic carbon content</i>	continuous	weight -%	697	8	QRF	-	-	0.339	0.77	91.32
<i>Sediment accumulation rate</i>	continuous	cm yr ⁻¹	220	8	QRF	-	-	0.135	0.32	88.19

347 ¹Model information relates to the additive log-ratio model.

348 4.2 Substantial amounts of organic carbon are stored in continental margin sediments

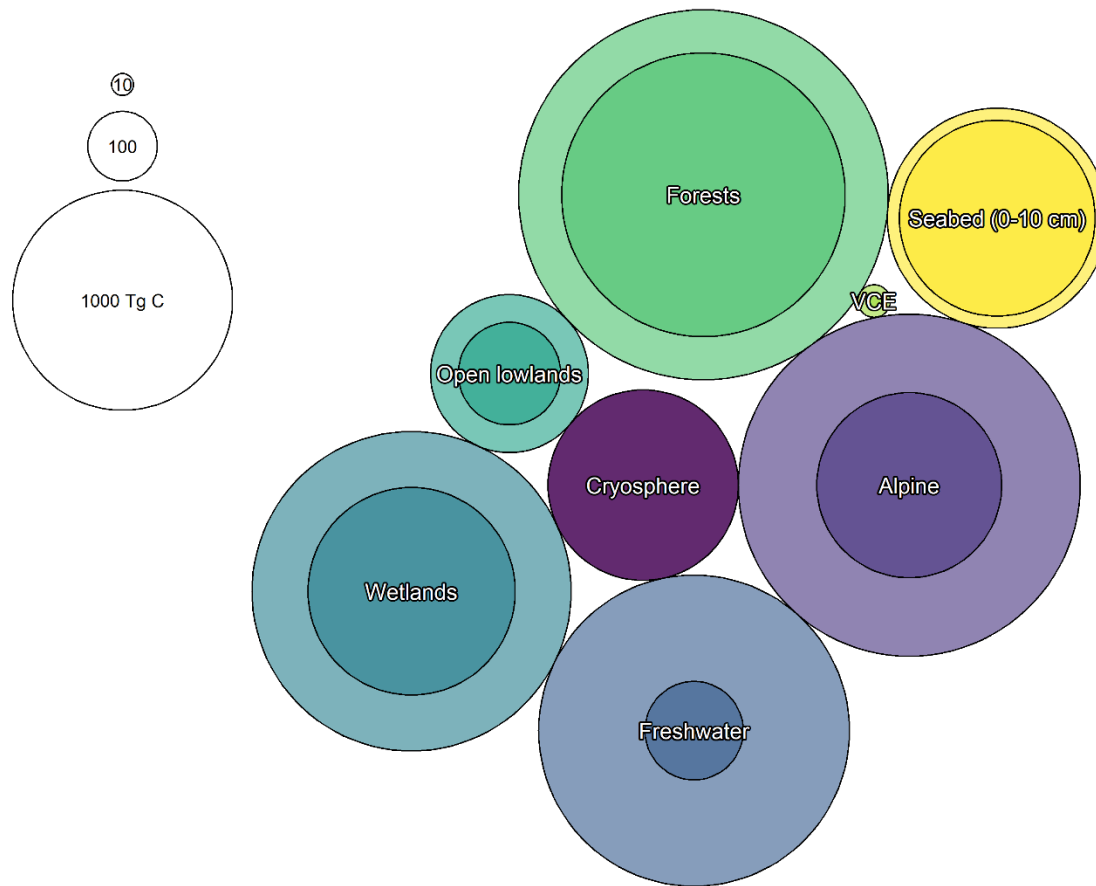
349 Organic carbon stocks of the upper 0.1 m of seafloor sediments range between 0.11 and
 350 3.34 kg m⁻², while the uncertainty varies between 0.21 and 4.04 kg m⁻² (Figure 2). Stocks are
 351 lowest (<0.5 kg m⁻²) on the North Sea shelf, shelf banks in the Norwegian Sea, along the shelf
 352 edge and slope foot and in parts of the southern Barents Sea. Conversely, stocks are highest
 353 (>2 kg m⁻²) off the northern and western coasts of Svalbard and in a southwest-northeast oriented
 354 band from Spitsbergen Bank to Central Bank. However, the calculated stocks on Spitsbergen
 355 Bank lie outside the joint area of applicability of the organic carbon and dry bulk density models
 356 and might be unrealistic, as coarse sediments (Bjørlykke et al., 1978) and mobile bedforms
 357 (Bellec et al., 2019) are widespread on the bank (Figures S1 and S2). Interestingly, the highest
 358 stocks as described above are located north of the marginal ice zone (Figure 2). In the seasonally
 359 sea ice covered northern area, higher stocks could reflect a highly variable primary production
 360 regime with efficient vertical export and less recycling than in the southern Barents Sea. Indeed,
 361 measured accumulation rates of organic carbon here are more than twice as high as in the ice-
 362 free southern region (Faust et al., 2020) reflecting the modern ecosystem with higher primary
 363 productivity but lower vertical organic flux rates in the southern than in the northern Barents Sea.

364 In addition, sea-ice induced lateral transport and subsequent release of terrestrial organic carbon
 365 can further accelerate deposition of primary produced organic carbon in the marginal ice zone
 366 (Knies & Martinez, 2009). Shelf valleys tend to have higher organic carbon stocks than their
 367 surrounding areas. This contrast is particularly stark between the Norwegian Trough and the
 368 North Sea shelf, indicating that shelf sediments can act in distinctly different ways in the context
 369 of organic carbon processing (Diesing et al., 2021). Indeed, centres of organic carbon
 370 accumulation and oxidation (Bianchi et al., 2018) might lie in close proximity to each other.



371
 372 **Figure 2.** Organic carbon stocks of surficial (0 – 10 cm) sediments on the Norwegian continental
 373 margin. Stocks were calculated from predicted dry bulk densities (Figure S4) and organic carbon
 374 contents (Figure S5). Left - Estimated organic carbon stocks (kg C m⁻²). MIZ – marginal ice zone
 375 based on Itkin et al. (2014). Centre – Prediction uncertainty (kg m⁻²), expressed as the 90%
 376 prediction interval. Right – Joint area of applicability (AOA) of the models. Areas predicted as
 377 rock in the substrate type model (Figure S1) were excluded from the analysis.

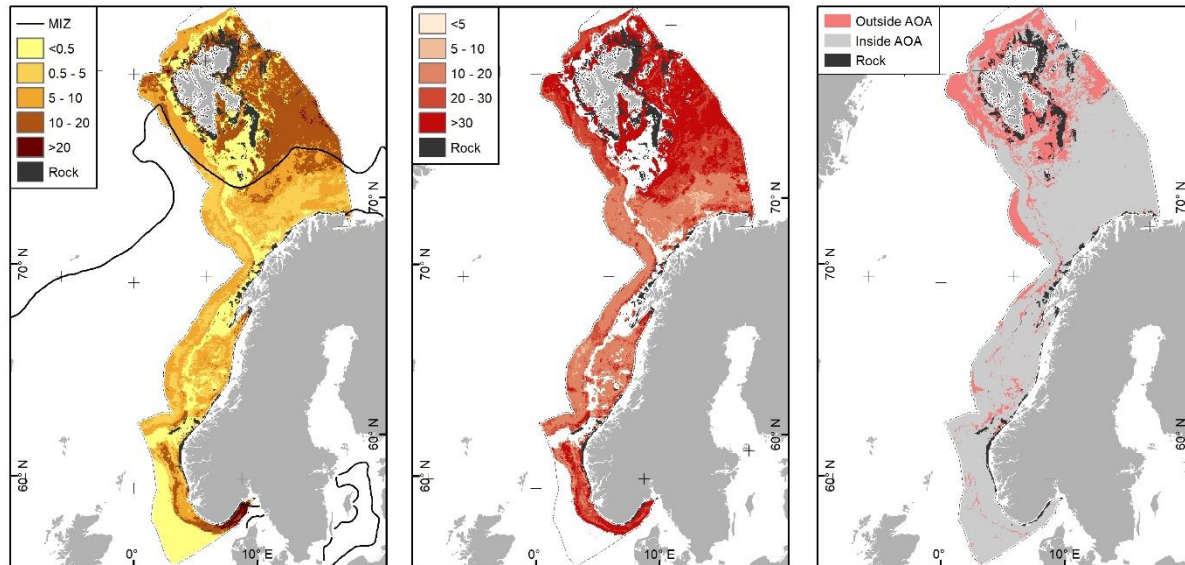
378
 379 The reservoir size of margin sediments in Norway was calculated to $1,002 \pm 1,485$ Tg C within
 380 the area of interest and $793 \pm 1,152$ Tg C within the joint area of applicability. By comparison,
 381 current best estimates of reservoir sizes in vegetated coastal ecosystems (salt marshes, eelgrass
 382 meadows and brown macroalgae) in the Nordic countries (Greenland, Iceland, Faroe Islands,
 383 Norway, Denmark, Sweden, and Finland) amount to 9.26 Tg C (Krause-Jensen et al., 2022). The
 384 organic carbon reservoir size of vegetated coastal ecosystems in Norway has been estimated to
 385 be 5 – 22 Tg C (Bartlett et al., 2020). Continental margin sediments thus store approximately two
 386 orders of magnitude more organic carbon than coastal vegetated ecosystems, even though we
 387 have only considered the upper 0.1 m of the sediment column while other estimates typically
 388 refer to the upper 1 m (Figure 3). Reservoir sizes of margin sediments might even be comparable
 389 to terrestrial ecosystems such as forest soils (1,240 – 1,830 Tg C) and wetlands (890 –
 390 2,089 Tg C) in Norway (Bartlett et al., 2020). Despite the remaining uncertainties in the
 391 estimates, it would appear that continental margin sediments store substantial amounts of organic
 392 carbon and have so far been overlooked in the context of Blue Carbon.



393
 394 **Figure 3.** Comparison of various organic carbon reservoir sizes in Norway: Surficial seabed
 395 sediments harbour between 793 Tg C (inside the AOA) and 1002 Tg C (inside and outside
 396 AOA). The reservoir size of vegetated coastal ecosystems (VCE) is much smaller (5 – 22 Tg C).
 397 Surficial seabed sediments have organic carbon reservoir sizes comparable to several terrestrial
 398 ecosystems such as wetlands and forests. Inner circles depict lower limit and outer circles upper
 399 limit of the estimated range of values. Data on Blue Carbon and terrestrial ecosystems are taken
 400 from Bartlett et al. (2020).

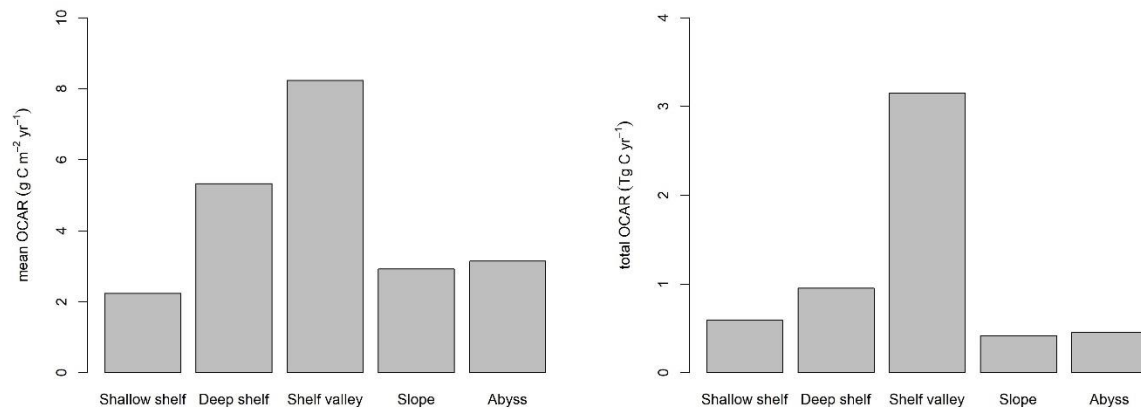
401 4.3 Complex patterns of organic carbon accumulation

402 As we used ^{210}Pb -derived sediment accumulation rates, the following estimates refer to
 403 accumulation over the last 100 - 150 yr based on its half-life of 22.2 yr and an integration time of
 404 approximately five to seven times the half-life (Goldberg, 1963).



405
 406 **Figure 4.** Organic carbon accumulation rates on the Norwegian continental margin. Organic
 407 carbon accumulation rates were calculated from organic carbon stocks of surficial (0 – 10 cm)
 408 sediments (Figure 2) and sediment accumulation rates (Figure S6). Left - Estimated organic
 409 carbon accumulation rates ($\text{g C m}^{-2} \text{yr}^{-1}$). MIZ – marginal ice zone based on Itkin et al. (2014).
 410 Centre – Prediction uncertainty ($\text{g C m}^{-2} \text{yr}^{-1}$), expressed as the 90% prediction interval. Note that
 411 the uncertainty is not defined in areas with sedimentation rates of 0 cm yr^{-1} (see equation 7).
 412 Right – Joint area of applicability of the models. Areas predicted as rock in the substrate type
 413 model (Figure S1) were excluded from the analysis.

414
 415 Organic carbon accumulation rates range from 0.0 to $106.4 \text{ g C m}^{-2} \text{yr}^{-1}$, with uncertainties
 416 varying between 2.4 and $264.7 \text{ g C m}^{-2} \text{yr}^{-1}$ (Figure 4). Zero-accumulation of organic carbon is
 417 linked to the North Sea shelf, the shelf break, shelf banks in the Norwegian Sea, and Spitsbergen
 418 Bank, the latter in agreement with Pathirana et al. (2014). The main hotspot of organic carbon
 419 accumulation is to be found in the inner part of the Norwegian Trough in the Skagerrak.
 420 Additionally, elevated rates of organic carbon accumulation are widespread in the Barents Sea
 421 north of the marginal ice zone. However, calculated organic carbon accumulation rates lie
 422 outside the joint area of applicability of the organic carbon, dry bulk density and sediment
 423 accumulation models around Svalbard and on Spitsbergen Bank. Again, geomorphology acts as a
 424 major driver of the patterns of organic carbon accumulation. Depressions like shelf valleys act as
 425 centres of organic carbon accumulation due to high sedimentation rates (Figure S6), while
 426 shallow banks and plateaus show no accumulation at all due to their erosional character (Figure
 427 S2). The shelf edge shows no accumulation of organic carbon due to relatively strong currents
 428 preventing sediments and organic carbon from long-term accumulation. Conversely, the slope
 429 and upper part of the abyss are places of organic carbon accumulation. These patterns are also
 430 reflected in the mean organic carbon accumulation rates of geomorphological units: Mean rates
 431 are lowest on the shallow continental shelf ($2.24 \text{ g C m}^{-2} \text{yr}^{-1}$), which includes banks and
 432 plateaus, and highest in shelf valleys ($8.23 \text{ g C m}^{-2} \text{yr}^{-1}$), where they are nearly four times higher
 433 than on the inner shelf (Figure 5a). Elevated mean rates are also to be found on the deep
 434 continental shelf ($5.33 \text{ g C m}^{-2} \text{yr}^{-1}$), while slopes and the abyss exhibit moderate mean rates of
 435 $2.92 \text{ g C m}^{-2} \text{yr}^{-1}$ and $3.15 \text{ g C m}^{-2} \text{yr}^{-1}$, respectively.



436

437 **Figure 5.** Organic carbon accumulation rates of the geomorphological units as shown in Figure
 438 1. Left – Mean organic carbon accumulation rates averaged over the five morphological units.
 439 Right – Total organic carbon accumulation, i.e., mean rates multiplied by area.

440

441 Aggregated over the area of interest, the sediments of the Norwegian continental margin
 442 accumulate 7.5 ± 24.7 Tg C yr⁻¹. Restricted to the joint area of applicability, organic carbon
 443 accumulation amounts to 5.6 ± 18.1 Tg C yr⁻¹. For comparison, coastal vegetated ecosystems
 444 might accumulate 0.55 Tg C yr⁻¹ in the Nordic countries (Krause-Jensen et al., 2022) and 0.25 –
 445 0.37 Tg C yr⁻¹ in Norway (Bartlett et al., 2020). Expressed in equivalents of CO₂, Norwegian
 446 margin sediments accumulate 20.6 Tg CO₂-eq per year within the joint area of applicability. This
 447 is equivalent to 42% of Norway’s greenhouse gas emissions of 48.9 Tg CO₂-eq in 2022 (SSB,
 448 2023).

449 More than half of the accumulation of organic carbon is happening in shelf valleys (Figure 5b)
 450 due to their high accumulation rates per unit area (Figure 5a) and the large areas they occupy on
 451 the Norwegian continental margin (Figure 1), amounting to 388,288 km². Shelf valleys are
 452 therefore centres of organic carbon accumulation on the Norwegian continental margin. Most of
 453 these geomorphological features are of glacial origin and could also be described as glacial
 454 troughs attributed to glacial erosion during the Pleistocene ice ages. Globally, glacial troughs are
 455 found on the formerly glaciated continental margins of North America, Eurasia, south America,
 456 and Antarctica, covering 3.66 million km² of the seabed (Harris et al., 2014). If we assume that
 457 the rate of organic carbon accumulation in shelf valleys of 8.23 g C m⁻² yr⁻¹ we derived is
 458 representative for glacial troughs globally, then these geomorphological features might
 459 accumulate 30 Tg C yr⁻¹, which is comparable to fjords (21 – 25 Tg C/yr; Smith et al., 2015),
 460 seagrass meadows (14.7 - 27.4 Tg C/yr; Duarte et al., 2005; Taillardat et al., 2018), mangroves
 461 (13.5 - 26.1 Tg C/yr; Alongi, 2012; Breithaupt et al., 2012; Taillardat et al., 2018), and
 462 saltmarshes (10.1 - 10.2 Tg C/yr; Ouyang & Lee, 2014; Taillardat et al., 2018). Although our
 463 global estimate is currently tentative, it points to a hitherto overlooked environment with high
 464 potential for organic carbon accumulation.

465 4.4 Towards a global map of organic carbon accumulation rates

466 Previous estimates of organic carbon burial in seafloor sediments of the global ocean have
 467 frequently been non-spatial and only Burdige (2007) considered that large parts of continental

468 margins do not accumulate sediment and organic carbon (de Haas et al., 2002). Moreover,
469 assumptions about how much organic carbon that is accumulated at the seafloor gets eventually
470 buried are frequently very general. For example, Berner (1982) assumed a preservation rate of
471 80% globally. Estimated organic carbon fluxes based on satellite data (Dunne et al., 2007;
472 Muller-Karger et al., 2005) gave spatially explicit results, but also had to make assumptions
473 about the burial efficiency, e.g., Muller-Karger et al. (2005) assumed burial efficiencies of 30%
474 in the deep sea and 10% on margins. Moreover, such studies were not able to resolve the spatial
475 complexities of continental margin processes, as they implicitly assumed a static ocean where
476 organic matter sinks to the seafloor and resuspension, erosion and transport had little effect.
477 Consequently, these studies estimated high rates of organic carbon burial across all margins.
478 Because of the vague definition of organic carbon burial (see the discrepancies between the
479 values of burial efficiency cited above and Bradley et al. (2022)), we decided to estimate organic
480 carbon accumulation rates instead. These are representative of the last 100 to 150 years, i.e., the
481 time interval since the start of the industrial revolution and the increase of anthropogenic CO₂
482 emissions due to the burning of fossil fuels. We were also able to account for the complex nature
483 of the Norwegian continental margin in terms of sediment erosion and deposition because the
484 depositional environment is being mapped as part of the Mareano programme.
485 Unlike organic carbon content (Lee et al., 2019) and stocks (Atwood et al., 2020), organic carbon
486 accumulation rates have not been mapped globally with machine learning approaches. To do so
487 will require a) data on organic carbon content, dry bulk density and sediment accumulation rates
488 of sufficient quality and quantity, b) relevant predictor variables of global coverage and
489 sufficient resolution, and c) spatial models that take into account the complex nature of
490 continental margins, where centres of organic carbon accumulation and cycling might be found
491 in close proximity to each other (Diesing et al., 2021; de Haas et al., 2002). While progress has
492 been made to make relevant response (Felden et al., 2023; Paradis et al., 2023) and predictor
493 variables (Assis et al., 2018) available, there are still several obstacles that need to be overcome.
494 We consider the lack of a global map of the depositional environment as the main obstacle on a
495 path towards a global map of organic carbon accumulation rates. Burdige (2007) used Emery's
496 (1968) map of relict sediments on the continental shelves of the global ocean as a proxy.
497 However, this map does not exist electronically, might be outdated by now and is not explicitly
498 depicting the depositional environment. The first task would therefore be to predict the
499 depositional environment on continental margins globally.

500 **5 Conclusions**

501 We spatially predicted dry bulk density, organic carbon content and sediment accumulation rates
502 of surface sediments on the continental margin of Norway to estimate organic carbon stocks and
503 accumulation rates. Organic carbon reservoirs are two orders of magnitude larger than those of
504 vegetated coastal ecosystems in Norway, even if we only considered the upper ten centimetres of
505 the sediment column. Rates of organic carbon accumulation are spatially highly variable and
506 highest in shelf valleys of mostly glacial origin. Considering the global extension of glacial
507 troughs in the global ocean, these geomorphologic features might be accumulating as much
508 organic carbon as fjords, seagrass meadows, mangroves, and saltmarshes. Global spatial
509 predictions of sediment and organic carbon accumulation rates are required for a better
510 understanding of the role of margin sediments in the carbon cycle and to evaluate whether
511 continental margin sediments constitute actionable Blue Carbon ecosystems.

512 Acknowledgments

513 This work was funded by the Norwegian seabed mapping programme Mareano. JK received
514 support from the Research Council of Norway (grant # 332635).

515 Conflict of interest

517 The authors declare no conflict of interest.

518 Open Research

519 Calculated organic carbon stocks and accumulation rates and the related uncertainties and areas
520 of applicability are available from PANGAEA: [*Insert doi when minted*]
521 Input (response and predictor variables) and output data of the six spatial models are available at
522 Zenodo. The R codes developed to spatially predict the response variables are available at
523 GitHub.

524
525 *NB! Data on Zenodo and PANGAEA have been created but not yet published. The datasets have*
526 *been made available for peer review.*

527

Variable	Input data	Output data	R workflow
Substrate type	https://doi.org/10.5281/zenodo.10040165	https://doi.org/10.5281/zenodo.10053285	https://github.com/diesingngu/GrainSizeReg
Depositional environment	https://doi.org/10.5281/zenodo.10040720	https://doi.org/10.5281/zenodo.10053457	https://github.com/diesingngu/SedEnv
Mud content	https://doi.org/10.5281/zenodo.10057143	https://doi.org/10.5281/zenodo.10057207	https://github.com/diesingngu/GSMgrids
Dry bulk density	https://doi.org/10.5281/zenodo.10057726	https://doi.org/10.5281/zenodo.10057750	https://github.com/diesingngu/DBD
Organic carbon content	https://doi.org/10.5281/zenodo.10058434	https://doi.org/10.5281/zenodo.10058520	https://github.com/diesingngu/TOC
Sediment accumulation rate	https://doi.org/10.5281/zenodo.10061180	https://doi.org/10.5281/zenodo.10062619	https://github.com/diesingngu/SedRates

528

529 References

- 530 Alongi, D. M. (2012). Carbon sequestration in mangrove forests. *Carbon Management*, 3(3), 313–322.
531 <https://doi.org/10.4155/cmt.12.20>
- 532 Arrouays, D., Grundy, M. G., Hartemink, A. E., Hempel, J. W., Heuvelink, G. B. M., Hong, S. Y., et al. (2014).
533 Chapter Three - GlobalSoilMap: Toward a Fine-Resolution Global Grid of Soil Properties. In D. L. Sparks
534 (Ed.) (Vol. 125, pp. 93–134). Academic Press. [https://doi.org/https://doi.org/10.1016/B978-0-12-800137-](https://doi.org/https://doi.org/10.1016/B978-0-12-800137-0.00003-0)
535 [0.00003-0](https://doi.org/10.1016/B978-0-12-800137-0.00003-0)
- 536 Assis, J., Tyberghein, L., Bosch, S., Verbruggen, H., Serrão, E. A., & De Clerck, O. (2018). Bio-ORACLE v2.0:
537 Extending marine data layers for bioclimatic modelling. *Global Ecology and Biogeography*, 27(3), 277–284.
538 <https://doi.org/10.1111/geb.12693>
- 539 Atwood, T. B., Witt, A., Mayorga, J., Hammill, E., & Sala, E. (2020). Global Patterns in Marine Sediment Carbon
540 Stocks. *Frontiers in Marine Science*, 7, 165. <https://doi.org/10.3389/fmars.2020.00165>
- 541 Bartlett, J., Rusch, G. M., Kyrkjeeide, M. O., Sandvik, H., & Nordén, J. (2020). Carbon storage in Norwegian
542 ecosystems (revised edition). *NINA Report, 1774b*. Retrieved from <https://hdl.handle.net/11250/2655580>
- 543 Bellec, V. K., Bøe, R., Bjarnadóttir, L. R., Albretsen, J., Dolan, M., Chand, S., et al. (2019). Sandbanks, sandwaves
544 and megaripples on Spitsbergenbanken, Barents Sea. *Marine Geology*, 416, 105998.
545 <https://doi.org/https://doi.org/10.1016/j.margeo.2019.105998>
- 546 Berner, R. A. (1982). Burial of organic carbon and pyrite sulfur in the modern ocean: Its geochemical and
547 environmental significance. *American Journal of Science*, 282, 451–473. <https://doi.org/10.2475/ajs.282.4.451>

- 548 Berner, R. A. (2003). The long-term carbon cycle, fossil fuels and atmospheric composition. *Nature*, *426*, 323.
549 Retrieved from <https://doi.org/10.1038/nature02131>
- 550 Bianchi, T. S., Cui, X., Blair, N. E., Burdige, D. J., Eglinton, T. I., & Galy, V. (2018). Centers of organic carbon
551 burial and oxidation at the land-ocean interface. *Organic Geochemistry*, *115*, 138–155.
552 <https://doi.org/https://doi.org/10.1016/j.orggeochem.2017.09.008>
- 553 Bjørlykke, K., Bue, B., & Elverhøi, A. (1978). Quaternary sediments in the northwestern part of the Barents Sea and
554 their relation to the underlying Mesozoic bedrock. *Sedimentology*, *25*(2), 227–246.
555 <https://doi.org/https://doi.org/10.1111/j.1365-3091.1978.tb00310.x>
- 556 Bøe, R., Rise, L., Thorsnes, T., de Haas, H., Sæther, O. M., & Kunzendorf, H. (1996). Sea-bed sediments and
557 sediment accumulation rates in the Norwegian part of the Skagerrak. *NGU Bulletin*, *430*, 75–84.
- 558 Bradley, J. A., Hülse, D., LaRowe, D. E., & Arndt, S. (2022). Transfer efficiency of organic carbon in marine
559 sediments. *Nature Communications*, *13*(1), 7297. <https://doi.org/10.1038/s41467-022-35112-9>
- 560 Breiman, L. (2001). Random Forests. *Machine Learning*, *45*, 5–32.
561 <https://doi.org/https://doi.org/10.1023/A:1010933404324>
- 562 Breithaupt, J. L., Smoak, J. M., Smith III, T. J., Sanders, C. J., & Hoare, A. (2012). Organic carbon burial rates in
563 mangrove sediments: Strengthening the global budget. *Global Biogeochemical Cycles*, *26*(3).
564 <https://doi.org/https://doi.org/10.1029/2012GB004375>
- 565 Burdige, D. J. (2007). Preservation of Organic Matter in Marine Sediments: Controls, Mechanisms, and an
566 Imbalance in Sediment Organic Carbon Budgets? *Chemical Reviews*, *107*(2), 467–485.
567 <https://doi.org/10.1021/cr050347q>
- 568 Congalton, R. G. (1991). A review of assessing the accuracy of classifications of remotely sensed data. *Remote
569 Sensing of Environment*, *37*(1), 35–46. Retrieved from
570 <http://www.sciencedirect.com/science/article/pii/003442579190048B>
- 571 Diesing, M., Kröger, S., Parker, R., Jenkins, C., Mason, C., & Weston, K. (2017). Predicting the standing stock of
572 organic carbon in surface sediments of the North–West European continental shelf. *Biogeochemistry*, *135*(1–
573 2), 183–200. <https://doi.org/10.1007/s10533-017-0310-4>
- 574 Diesing, M., Thorsnes, T., & Bjarnadóttir, L. R. (2021). Organic carbon densities and accumulation rates in surface
575 sediments of the North Sea and Skagerrak. *Biogeosciences*, *18*(6), 2139–2160. [https://doi.org/10.5194/bg-18-
576 2139-2021](https://doi.org/10.5194/bg-18-2139-2021)
- 577 DNV. (2023). Environmental Monitoring database (MOD) DNV. <https://doi.org/https://doi.org/10.15468/q8qykg>
- 578 Duarte, C. M., Middelburg, J. J., & Caraco, N. (2005). Major role of marine vegetation on the oceanic carbon cycle.
579 *Biogeosciences*, *2*(1), 1–8. <https://doi.org/10.5194/bg-2-1-2005>
- 580 Duarte, C. M., Losada, I. J., Hendriks, I. E., Mazarrasa, I., & Marbà, N. (2013). The role of coastal plant
581 communities for climate change mitigation and adaptation. *Nature Climate Change*, *3*(11), 961–968.
582 <https://doi.org/10.1038/nclimate1970>
- 583 Dunne, J. P., Sarmiento, J. L., & Gnanadesikan, A. (2007). A synthesis of global particle export from the surface
584 ocean and cycling through the ocean interior and on the seafloor. *Global Biogeochemical Cycles*, *21*(4).
585 <https://doi.org/https://doi.org/10.1029/2006GB002907>
- 586 Emery, K. O. (1968). Relict sediments on continental shelves of world. *American Association of Petroleum
587 Geologists Bulletin*, *52*(3), 445–464.
- 588 Faust, J. C., Stevenson, M. A., Abbott, G. D., Knies, J., Tessin, A., Mannion, I., et al. (2020). Does Arctic warming
589 reduce preservation of organic matter in Barents Sea sediments? *Philosophical Transactions of the Royal
590 Society A: Mathematical, Physical and Engineering Sciences*, *378*(2181), 20190364.
591 <https://doi.org/10.1098/rsta.2019.0364>
- 592 Felden, J., Möller, L., Schindler, U., Huber, R., Schumacher, S., Koppe, R., et al. (2023). PANGAEA - Data
593 Publisher for Earth & Environmental Science. *Scientific Data*, *10*(1), 347. [https://doi.org/10.1038/s41597-023-
594 02269-x](https://doi.org/10.1038/s41597-023-02269-x)
- 595 Folk, R. L. (1954). The distinction between grain size and mineral composition in sedimentary-rock nomenclature.
596 *Journal of Geology*, *62*, 344–359.
- 597 GEBCO Bathymetric Compilation Group. (2019). The GEBCO_2019 Grid - a continuous terrain model of the
598 global oceans and land. <https://doi.org/10.5285/836f016a-33be-6ddc-e053-6c86abc0788e>
- 599 Goldberg, E. D. (1963). Geochronology with Pb-210. In *Radioactive Dating. Proceedings of the Symposium on
600 Radioactive Dating Held by the International Atomic Energy Agency in Co-operation with the Joint
601 Commission on Applied Radioactivity* (pp. 121–131). Athens.
- 602 de Haas, H., Boer, W., & van Weering, T. C. E. (1997). Recent sedimentation and organic carbon burial in a shelf
603 sea: the North Sea. *Marine Geology*, *144*, 131–146. [https://doi.org/10.1016/S0025-3227\(97\)00082-0](https://doi.org/10.1016/S0025-3227(97)00082-0)

- 604 de Haas, H., van Weering, T. C. E., & de Stigter, H. (2002). Organic carbon in shelf seas: sinks or sources, processes
605 and products. *Continental Shelf Research*, 22(5), 691–717. [https://doi.org/10.1016/S0278-4343\(01\)00093-0](https://doi.org/10.1016/S0278-4343(01)00093-0)
- 606 Harris, P. T., Macmillan-Lawler, M., Rupp, J., & Baker, E. K. (2014). Geomorphology of the oceans. *Marine*
607 *Geology*, 352, 4–24. <https://doi.org/10.1016/j.margeo.2014.01.011>
- 608 Hedges, J. I., & Keil, R. G. (1995). Sedimentary organic matter preservation: an assessment and speculative
609 synthesis. *Marine Chemistry*, 49(2–3), 81–115. [https://doi.org/10.1016/0304-4203\(95\)00008-F](https://doi.org/10.1016/0304-4203(95)00008-F)
- 610 Hengl, T. (2006). Finding the right pixel size. *COMPUTERS & GEOSCIENCES*, 32, 1283–1298.
- 611 Hengl, T., de Jesus, J., Heuvelink, G. B. M., Ruiperez Gonzalez, M., Kilibarda, M., Blagotić, A., et al. (2017).
612 SoilGrids250m: Global gridded soil information based on machine learning. *PLOS ONE*, 12(2), 1–40.
613 <https://doi.org/10.1371/journal.pone.0169748>
- 614 Heuvelink, G. B. M. (2014). Uncertainty quantification of GlobalSoilMap products. Retrieved from
615 <https://api.semanticscholar.org/CorpusID:132005407>
- 616 Hiemstra, P. H., Pebesma, E. J., Twenhöfel, C. J. W., & Heuvelink, G. B. M. (2009). Real-time automatic
617 interpolation of ambient gamma dose rates from the Dutch radioactivity monitoring network. *Computers &*
618 *Geosciences*, 35(8), 1711–1721. <https://doi.org/https://doi.org/10.1016/j.cageo.2008.10.011>
- 619 Howard, J., Sutton-Grier, A. E., Smart, L. S., Lopes, C. C., Hamilton, J., Kleypas, J., et al. (2023). Blue carbon
620 pathways for climate mitigation: Known, emerging and unlikely. *Marine Policy*, 156, 105788.
621 <https://doi.org/https://doi.org/10.1016/j.marpol.2023.105788>
- 622 Huang, Z., Siwabessy, J., Nichol, S. L., & Brooke, B. P. (2014). Predictive mapping of seabed substrata using high-
623 resolution multibeam sonar data: A case study from a shelf with complex geomorphology. *Marine Geology*,
624 357, 37–52. Retrieved from <http://www.sciencedirect.com/science/article/pii/S0025322714002205>
- 625 Hunt, C., Demšar, U., Dove, D., Smeaton, C., Cooper, R., & Austin, W. E. N. (2020). Quantifying Marine
626 Sedimentary Carbon: A New Spatial Analysis Approach Using Seafloor Acoustics, Imagery, and Ground-
627 Truthing Data in Scotland. *Frontiers in Marine Science*, 7, 588. <https://doi.org/10.3389/fmars.2020.00588>
- 628 Itkin, M., Konig, M., Spreen, G., & Vongraven, D. (2014). Arctic sea ice frequency with maximum and minimum
629 extentw. <https://doi.org/10.21334/npolar.2014.a89b2682>
- 630 Jenkins, C. (2005). Summary of the onCALCULATION methods used in dbSEABED. Retrieved September 2,
631 2016, from <http://pubs.usgs.gov/ds/2006/146/docs/onCALCULATION.pdf>
- 632 Jenkins, C. (2018). Sediment Accumulation Rates For the Mississippi Delta Region: a Time-interval Synthesis.
633 *Journal of Sedimentary Research*, 88(2), 301–309. <https://doi.org/10.2110/jsr.2018.15>
- 634 Johnston, R., Jones, K., & Manley, D. (2018). Confounding and collinearity in regression analysis: a cautionary tale
635 and an alternative procedure, illustrated by studies of British voting behaviour. *Quality & Quantity*, 52(4),
636 1957–1976. <https://doi.org/10.1007/s11135-017-0584-6>
- 637 Keil, R. (2017). Anthropogenic Forcing of Carbonate and Organic Carbon Preservation in Marine Sediments.
638 *Annual Review of Marine Science*, 9(1), 151–172. <https://doi.org/10.1146/annurev-marine-010816-060724>
- 639 Knies, J., & Martinez, P. (2009). Organic matter sedimentation in the western Barents Sea region: Terrestrial and
640 marine contribution based on isotopic composition and organic nitrogen content. *Norwegian Journal of*
641 *Geology*, 89, 79–89.
- 642 Krause-Jensen, D., Gundersen, H., Björk, M., Gullström, M., Dahl, M., Asplund, M. E., et al. (2022). Nordic Blue
643 Carbon Ecosystems: Status and Outlook. *Frontiers in Marine Science*, 9,
644 <https://doi.org/10.3389/fmars.2022.847544>
- 645 Kursa, M. B., & Rudnicki, W. R. (2010). Feature Selection with the **Boruta** Package. *Journal of Statistical*
646 *Software*, 36(11), 1–13. <https://doi.org/10.18637/jss.v036.i11>
- 647 Lee, T. R., Wood, W. T., & Phrampus, B. J. (2019). A Machine Learning (kNN) Approach to Predicting Global
648 Seafloor Total Organic Carbon. *Global Biogeochemical Cycles*, 33(1), 37–46.
649 <https://doi.org/10.1029/2018GB005992>
- 650 Legge, O., Johnson, M., Hicks, N., Jickells, T., Diesing, M., Aldridge, J., et al. (2020). Carbon on the Northwest
651 European Shelf: Contemporary Budget and Future Influences. *Frontiers in Marine Science*, 7, 143.
652 <https://doi.org/10.3389/fmars.2020.00143>
- 653 Lovelock, C. E., & Duarte, C. M. (2019). Dimensions of Blue Carbon and emerging perspectives. *Biology Letters*,
654 15(3), 20180781. <https://doi.org/10.1098/rsbl.2018.0781>
- 655 Luts, J., Ojeda, F., Plas, R., Van De Moor, B., De Huffel, S., & Van Suykens, J. A. K. (2010). A tutorial on support
656 vector machine-based methods for classification problems in chemometrics. *Analytica Chimica Acta*, 665(2),
657 129–145.

- 658 Martín-Fernandéz, J. A., & Thió-Henestrosa, S. (2006). Rounded zeros: some practical aspects for compositional
659 data. In A. Buccianti, G. Mateu-Figueras, & V. Pawlowsky-Glahn (Eds.), *Compositional Data Analysis in the*
660 *Geosciences: From Theory to Practice* (Vol. 264, pp. 191–201). Geological Society of London.
- 661 Meinshausen, N. (2006). Quantile Regression Forests. *Journal of Machine Learning Research*, 7, 983–999.
- 662 Meyer, H., & Pebesma, E. (2021). Predicting into unknown space? Estimating the area of applicability of spatial
663 prediction models. *Methods in Ecology and Evolution*, 12(9), 1620–1633.
664 <https://doi.org/https://doi.org/10.1111/2041-210X.13650>
- 665 Meyer, H., & Pebesma, E. (2022). Machine learning-based global maps of ecological variables and the challenge of
666 assessing them. *Nature Communications*, 13(1), 2208. <https://doi.org/10.1038/s41467-022-29838-9>
- 667 Meyer, H., Reudenbach, C., Hengl, T., Katurji, M., & Nauss, T. (2018). Improving performance of spatio-temporal
668 machine learning models using forward feature selection and target-oriented validation. *Environmental*
669 *Modelling & Software*, 101, 1–9. <https://doi.org/https://doi.org/10.1016/j.envsoft.2017.12.001>
- 670 Meyer, H., Mila, C., Ludwig, M., & Linnenbrink, J. (2023). CAST: “caret” applications for Spatial-Temporal
671 Models. <https://github.com/HannaMeyer/CAST>. Retrieved from <https://github.com/HannaMeyer/CAST>
- 672 Mitchell, P. J., Aldridge, J., & Diesing, M. (2019). Legacy data: How decades of seabed sampling can produce
673 robust predictions and versatile products. *Geosciences (Switzerland)*.
674 <https://doi.org/10.3390/geosciences9040182>
- 675 Mitchell, P. J., Spence, M. A., Aldridge, J., Kotilainen, A. T., & Diesing, M. (2021). Sedimentation rates in the
676 Baltic Sea: A machine learning approach. *Continental Shelf Research*, 214, 104325.
677 <https://doi.org/https://doi.org/10.1016/j.csr.2020.104325>
- 678 Muller-Karger, F. E., Varela, R., Thunell, R., Luerssen, R., Hu, C., & Walsh, J. J. (2005). The importance of
679 continental margins in the global carbon cycle. *Geophysical Research Letters*, 32(1).
680 <https://doi.org/https://doi.org/10.1029/2004GL021346>
- 681 Mutanga, O., Adam, E., & Cho, M. A. (2012). High density biomass estimation for wetland vegetation using
682 WorldView-2 imagery and random forest regression algorithm. *International Journal of Applied Earth*
683 *Observation and Geoinformation*, 18, 399–406. <https://doi.org/10.1016/j.jag.2012.03.012>
- 684 Naimi, B., Hamm, N. A. S., Groen, T. A., Skidmore, A. K., & Toxopeus, A. G. (2014). Where is positional
685 uncertainty a problem for species distribution modelling? *Ecography*, 37(2), 191–203.
686 <https://doi.org/https://doi.org/10.1111/j.1600-0587.2013.00205.x>
- 687 Nellemann, C., Corcoran, E., Duarte, C. M., Valdés, L., De Young, C., Fonseca, L., & Grimsditch, G. (2009). *Blue*
688 *Carbon: The Role of Healthy Oceans in Binding Carbon: A Rapid Response Assessment*. Environment.
- 689 Oliveira, S., Oehler, F., San-Miguel-Ayanz, J., Camia, A., & Pereira, J. M. C. (2012). Modeling spatial patterns of
690 fire occurrence in Mediterranean Europe using Multiple Regression and Random Forest. *Forest Ecology and*
691 *Management*, 275, 117–129. <https://doi.org/10.1016/j.foreco.2012.03.003>
- 692 Ouyang, X., & Lee, S. Y. (2014). Updated estimates of carbon accumulation rates in coastal marsh sediments.
693 *Biogeosciences*, 11(18), 5057–5071. <https://doi.org/10.5194/bg-11-5057-2014>
- 694 Paradis, S., Nakajima, K., der Voort, T. S., Gies, H., Wildberger, A., Blattmann, T. M., et al. (2023). The Modern
695 Ocean Sediment Archive and Inventory of Carbon (MOSAIC): version 2.0. *Earth System Science Data*, 15(9),
696 4105–4125. <https://doi.org/10.5194/essd-15-4105-2023>
- 697 Pathirana, I., Knies, J., Felix, M., & Mann, U. (2014). Towards an improved organic carbon budget for the western
698 Barents Sea shelf. *Climate of the Past*, 10(2), 569–587. <https://doi.org/10.5194/cp-10-569-2014>
- 699 Pawlowsky-Glahn, V., & Olea, R. A. (2004). *Geostatistical Analysis of Compositional Data*. New York: Oxford
700 University Press.
- 701 Ploton, P., Mortier, F., Réjou-Méchain, M., Barbier, N., Picard, N., Rossi, V., et al. (2020). Spatial validation reveals
702 poor predictive performance of large-scale ecological mapping models. *Nature Communications*, 11(1), 4540.
703 <https://doi.org/10.1038/s41467-020-18321-y>
- 704 Prasad, A. M., Iverson, L. R., & Liaw, A. (2006). Newer classification and regression tree techniques: Bagging and
705 random forests for ecological prediction. *Ecosystems*, 9(2), 181–199. <https://doi.org/10.1007/s10021-005-0054-1>
- 706
- 707 Roberts, D. R., Bahn, V., Ciuti, S., Boyce, M. S., Elith, J., Guillera-Arroita, G., et al. (2017). Cross-validation
708 strategies for data with temporal, spatial, hierarchical, or phylogenetic structure. *Ecography*, 40(8), 913–929.
709 <https://doi.org/10.1111/ecog.02881>
- 710 Smeaton, C., Hunt, C. A., Turrell, W. R., & Austin, W. E. N. (2021). Marine Sedimentary Carbon Stocks of the
711 United Kingdom’s Exclusive Economic Zone. *Frontiers in Earth Science*, 9, 50.
712 <https://doi.org/10.3389/feart.2021.593324>

- 713 Smith, R. W., Bianchi, T. S., Allison, M., Savage, C., & Galy, V. (2015). High rates of organic carbon burial in fjord
714 sediments globally. *Nature Geoscience*, 8(6), 450–453. <https://doi.org/10.1038/NGEO2421>
- 715 SSB. (2023). Emissions to air. Retrieved November 2, 2023, from <https://www.ssb.no/en/natur-og->
716 [miljo/forurensing-og-klima/statistikk/utslipp-til-luft](https://www.ssb.no/en/natur-og-miljo/forurensing-og-klima/statistikk/utslipp-til-luft)
- 717 Stephens, D., & Diesing, M. (2015). Towards quantitative spatial models of seabed sediment composition. *PLoS*
718 *ONE*, 10(11), e0142502. <https://doi.org/10.1371/journal.pone.0142502>
- 719 Taillardat, P., Friess, D. A., & Lupascu, M. (2018). Mangrove blue carbon strategies for climate change mitigation
720 are most effective at the national scale. *Biology Letters*, 14(10), 20180251.
721 <https://doi.org/10.1098/rsbl.2018.0251>
- 722 Valavi, R., Elith, J., Lahoz-Monfort, J. J., & Guillera-Aroita, G. (2019). blockCV: An r package for generating
723 spatially or environmentally separated folds for k-fold cross-validation of species distribution models.
724 *Methods in Ecology and Evolution*, 10(2), 225–232. <https://doi.org/10.1111/2041-210X.13107>
- 725 van der Voort, T. S., Blattmann, T. M., Usman, M., Montluçon, D., Loeffler, T., Tavagna, M. L., et al. (2020).
726 MOSAIC (Modern Ocean Sediment Archive and Inventory of Carbon): A (radio)carbon-centric database for
727 seafloor surficial sediments. *Earth System Science Data Discussions*, 2020, 1–27. <https://doi.org/10.5194/essd->
728 [2020-199](https://doi.org/10.5194/essd-2020-199)
- 729 Wilson, R. J., Speirs, D. C., Sabatino, A., & Heath, M. R. (2018). A synthetic map of the north-west European Shelf
730 sedimentary environment for applications in marine science. *Earth System Science Data*, 10(1), 109–130.
731 <https://doi.org/10.5194/essd-10-109-2018>
- 732